ULTRAHIGH-Q SILICA-ALN HYBRID DISK OPTOMECHANICAL MODULATOR

Donggyu B. Sohn, JunHwan Kim, and Gaurav Bahl
University of Illinois at Urbana Champaign, Urbana, IL, USA

ABSTRACT

We present a hybrid silica (SiO_2) and aluminum nitride (AlN) optomechanical disk resonator capable of efficient optical modulation over a wide range of wavelengths. Light from a waveguide is coupled to modes of the high-Q wedge-disk optical resonator while the AlN piezoelectric layer actuates mechanical vibrations in response to an RF stimulus, resulting in light modulation via dispersive and dissipative coupling. We experimentally demonstrate modulation at both 1550 nm and 780 nm wavelengths.

INTRODUCTION

Optical modulators are a key building block across a wide range of photonic microsystems. For instance, modulators operating at telecom wavelengths help encode communication signals optically and to perform signal-processing functions [1, 2, 3]. Recent efforts on developing chip-scale atomic clocks necessitates the development of modulators that operate at wavelengths of interest for probing cold atoms, e.g. the 780 nm D2 line of Rubidium. In this paper, we report the development of a hybrid optical modulator that supports modulation over a very wide range of wavelengths spanning from telecom to visible.

Two key parameters that determine the modulated sideband strength in a resonator-based optomechanical modulator are the optical Q-factor and the mechanical excitation amplitude. The governing equation for the sidebands generated through resonator frequency modulation (dispersive effect) can be expressed as

$$a_{\pm 1} = \left(\frac{gu}{j(\Delta_l \pm \Omega) + \kappa/2} \right) a_0 \qquad (1)$$

where $a_{\pm 1}$ are the complex amplitudes [dimensionless] of the first order upper (+) and lower (-) frequency sidebands within the resonator, u is the acoustic field amplitude [dimensionless], Ω is mechanical frequency [Hz], κ is optical mode linewidth [Hz] ($\kappa = 1/Q_{opt}$), g is optomechanical coupling coefficient [Hz], Δ_l is frequency detuning of the input laser from the center of the optical mode [Hz], and a_0 is pump laser field amplitude in the cavity [dimensionless]. The major variables describing the system are illustrated in Figure 1. As can be seen above, the sideband amplitude is proportional to acoustic field and intracavity pump field, which can be obtained through

$$u = \frac{A\sqrt{\eta_{em}}}{j\Delta_b + \Gamma/2} \qquad (2)$$

$$a_0 = \left(\frac{\sqrt{\kappa_{ex}}}{j\Delta_l + \kappa/2} \right) s_{in} \qquad (3)$$

Here, A is the input RF drive that actuates the mechanical mode [$1/Hz^{1/2}$], η_{em} is the electromechanical power transduction efficiency [dimensionless], Δ_b is the detuning of the RF drive wave from the peak of the acoustic resonance [Hz], Γ_b is the acoustic mode linewidth [Hz] ($\Gamma_b = 1/Q_{mech}$), s_{in} is input laser field within the waveguide [$1/Hz^{1/2}$], and κ_{ex} is the external optical loss rate due to coupling between the waveguide and the optical resonator [Hz]. The dimensionless fields a_i are defined as $(\hbar\omega/\epsilon)|a_i|^2 = |E_i|^2$ where $\hbar$ is the Planck constant, ω is optical frequency, ϵ is permittivity, and E_i is the associated electric field amplitude [V/m]. Similarly, s_{in} is defined as $\hbar\omega|s_{in}|^2 = P_{in}$ where P_{in} is input optical power [Watts] [4].

It can be seen from equation (1) that in the "resolved sideband regime" i.e. Ω >> κ, the modulated field amplitude improves linearly with increasing optical Q-factor [3]. To achieve a large mechanical excitation leading to obtain large optical modulation, an efficient electromechanical transducer and high Q-factor mechanical resonance are also required [5]. We are thus motivated to explore materials and designs that simultaneously optimize both parameters.

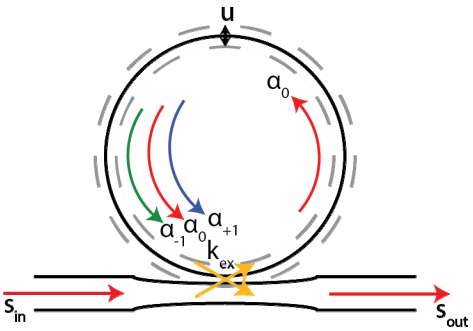

Figure 1: Description of variables used in the modulator equations.

DEVICE DESIGN

Our modulator is structured as a silica wedge optical resonator layered with an aluminum nitride disk having integrated aluminum transducers (IDTs). This stack of materials is supported on a silicon stem (Figure 2). We selected the chemically etched wedge-disk silica resonator structure since these can be prepared with extremely low

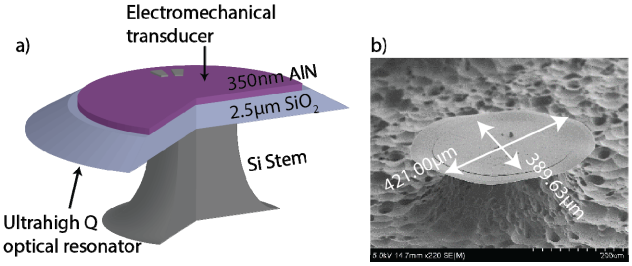

Figure 2: Schematic of the hybrid disk resonator; a) cross-section of with thickness of each layers b) tilted SEM image with disk dimension

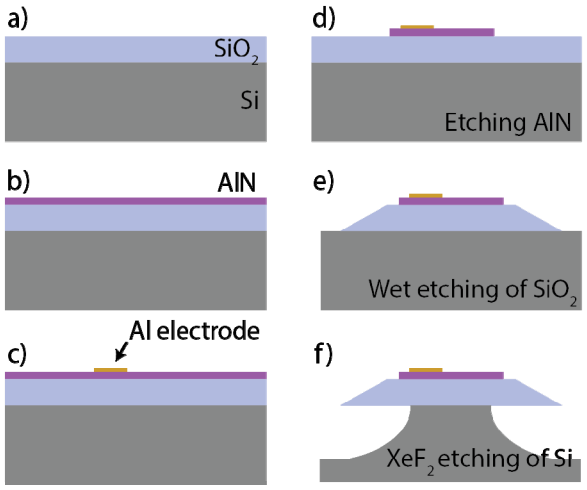

Figure 3: Fabrication process: (a) Substrate is 2.5 µm thermal SiO_2 on silicon substrate. (b) c-axis oriented AlN is deposited by sputtering. (c) Patterning of Al electrodes using lift off process. (d) AlN is etched using Cl_2 based ICP-RIE. (e) SiO_2 etched with BOE. (f) XeF_2 undercut to release the resonator edges.

surface roughness, have small intrinsic optical loss from absorption and defects, and can reach Q-factors in excess of 10^8 [6]. While the highest optical Q-factors have been reported with crystalline fluorides e.g. MgF_2 and CaF_2 [7], these materials are difficult to fabricate on-chip. Fused silica is a convenient high-Q alternative that allows easy integration with conventional materials and with nano-fabrication processes. The optical whispering gallery

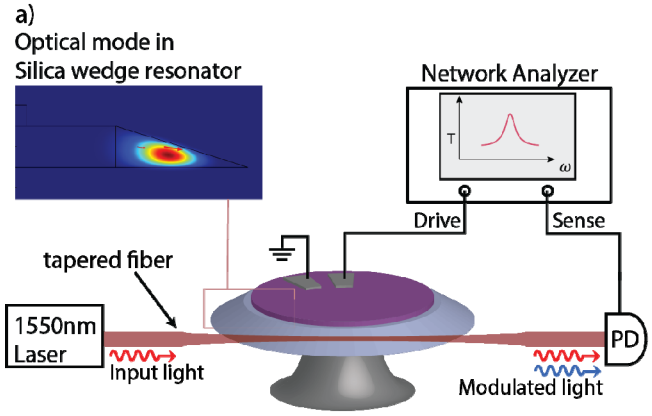

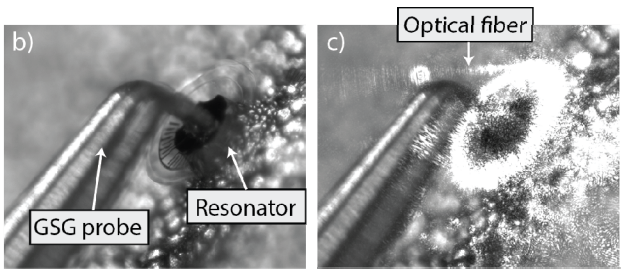

Figure 4: (a) Schematic of experimental test setup, showing the wedge optical mode as inset. (b) Microscope image of the hybrid disk resonator with GSG probe and optical tapered fiber. (c) With 780 nm source applied, the resonator and fiber are illuminated. Our camera is sensitive to 780 nm light.

modes in our resonators are confined near the edge of the disk such that the light does not interact with the AlN actuation layer. The IDTs are designed to maximize the electromechanical coupling with specific mechanical modes, which extend across both silica and AlN regions. Mechanical actuation modifies the optical path length around the disk, resulting in both amplitude modulation and dispersive modulation of the system [8].

FABRICATION

The fabrication process flow for this hybrid resonator system is shown in Figure 3. We deposited c-axis oriented AlN layer (commercially vendor OEM group) on a silicon wafer having 2.5 µm thermally grown SiO_2 layer. The quality of the AlN layer was confirmed using rocking curve x-ray measurement (FWHM 1.9 degree) and stress measurement (200 MPa). On the AlN layer, 60 nm thick aluminum interdigital transducers were patterned by standard lithography process followed by a lift off process. Next, the AlN disk was patterned and etched using Cl_2 based ICP-RIE. The circular optical resonator was patterned using standard photo-lithography on SPR-220 photoresist which was reflowed for 30 min at 120 °C to make a smooth circular structure. To ensure a smooth surface for the optical resonator, the SiO_2 was chemically etched using buffered oxide etchant. The angle of the wedge is set by the adhesion between SiO_2 and photoresist during BOE etching, which can be manipulated by use of different adhesion promoters. In our work, we used MCC primer from Microchem to achieve >15 degree wedge angle and to ensure high optical Q factor. Lastly, the edge of the resonator was released by XeF_2 vapor etching. Sufficient amount of the silicon was etched to ensure good electromechanical actuation efficiency as well as good optical confinement.

RESULT

We have experimentally demonstrated electro-opto-mechanical modulation using the hybrid disk resonator at both 780 nm and 1550 nm wavelength. Optical resonances are characterized using transmission measurements with a tapered optical fiber waveguide coupled to the resonator (Figure 4 and 5). The transmitted optical power is measured when the laser scans across the optical mode using a photodetector. The typical loaded optical quality

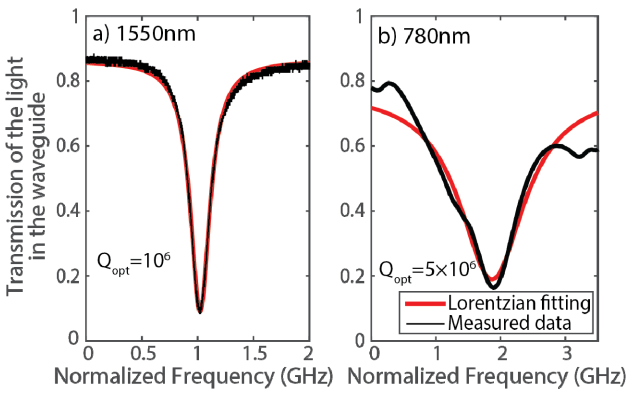

Figure 5: Optical resonance spectrum measured at (a) 1550 nm and (b) 780 nm.

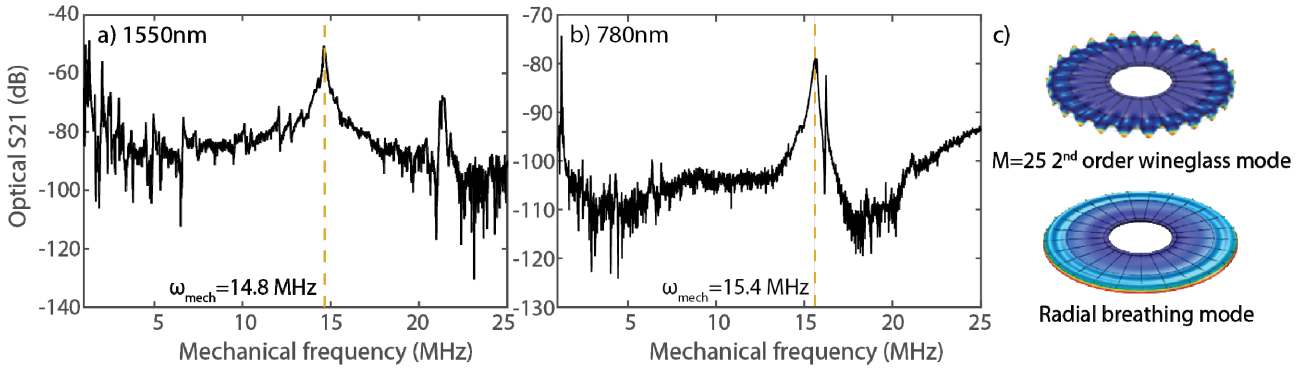

Figure 6: Measurement of the modulated light using optical S_{21} with a) 1550nm laser b) 780nm laser with the hybrid resonators in the same chip. The mechanical modes were detected at the frequencies of 14.8MHz and 15.4MHz respectively. c) Simulated possible mechanical modes corresponding to the measurement.

factor is measured to be ~10^6 at 1550 nm and 5×10^5 at 780 nm wavelength, validating that very high optical Q-factor can be achieved in the same device across very different wavelengths. An RF signal is delicately provided through a 50 µm pitch GSG probe directly onto the electrode layer (Figure 4b, c). For each measurement the laser was fixed at the -3 dB point of the optical resonance to obtain the largest modulation sidebands. The modulation of light was measured using a high-frequency photodetector while the mechanical mode was driven with an RF stimulus. Using a vector network analyzer, optical S_{21} parameter (the ratio of the beat note of measured by photodetector signal to the input RF signal) was measured in the frequency domain, which can expressed through the following equation

$$S_{21} = \left| \frac{2G\left| -s_{in} + \sqrt{\kappa_{ex}}\alpha_0 \right| \mathrm{Re}(\alpha_{+1} e^{-j\Omega t} + \alpha_{-1} e^{j\Omega t})}{A} \right| \quad (4)$$

Here, G is the photodetector gain. While the optical S_{21} parameter does not directly correspond to the modulation effectiveness, it does provide verification that optical modulation is taking place.

Measurements of the optical S_{21} parameter are presented in Figure 6 obtained during tests at the two wavelengths. The devices used for 780 nm and 1550 nm are physically different but were fabricated on the same chip. We observe a large electo-opto-mechanical response at mechanical resonances near 15 MHz. The optically measured quality factor of the mechanical mode with highest S_{21} parameter is 150. Several other mechanical modes are also seen in this measurement. The quality factor of some of these modes reaches up to 1600. Finite element simulations reveal that these mechanical modes may correspond either a 2nd radial order M=25 wineglass mechanical mode, or a high-order breathing mode (Figure 6c). The modes are not separable owing to their proximity in frequency. However, the high-order breathing mode is expected to have the highest S_{21} parameter with low mechanical Q-factor due to damping from the silicon stem.

CONCLUSION

In this work, we have presented the fabrication and testing of hybrid AlN-SiO_2 ultrahigh-Q disk resonators that enable large optomechanical coupling. As future work, a clearer identification of mechanical mode shape and improved IDT design to match the mechanical mode will improve the electromechanical coupling and optical modulation.

ACKNOWLEDGEMENTS

The authors would like to acknowledge a seedling grant from the DARPA Cold Atom Microsystems program (FA9453-16-1-0025) and an AFOSR Young Investigator grant (FA9550-15-1-0234).

REFERENCES

[1] S. Ghosh and G. Piazza, "Laterally vibrating resonator based elasto-optic modulation in aluminum nitride," *APL Photonics*, vol. 1, no. 3, p. 036101, 2016.

[2] S. Tallur and S. A. Bhave, "Electromechanically Induced GHz Rate Optical Frequency Modulation in Silicon," in IEEE Photonics Journal, vol. 4, no. 5, pp. 1474-1483, 2012

[3] H. Li, S. A. Tadesse, Q. Liu, and M. Li, "Nanophotonic cavity optomechanics with propagating acoustic waves at frequencies up to 12ghz," *Optica*, vol. 2, no. 9, pp. 826–831, 2015.

[4] G. S. Agarwal and S. S. Jha, "Multimode phonon cooling via three-wave parametric interactions with optical fields," Phys. Rev. A, vol. 88, p. 013815, 2013.

[5] G. Piazza, P. J. Stephanou, and A. P. Pisano, "Piezoelectric aluminum nitride vibrating contour-mode mems resonators," *JMEMS*, vol. 15, no. 6, pp. 1406–1418, 2006.

[6] H. Lee, T. Chen, J. Li, K. Y. Yang, S. Jeon, O. Painter, and K. J. Vahala, "Chemically etched ultrahigh-Q wedge-resonator on a silicon chip," *Nat Photon*, vol. 6, no. 6, pp. 369–373, 2012.

[7] I. S. Grudinin, V. S. Ilchenko, and L. Maleki, "Ultrahigh optical q factors of crystalline resonators in the linear regime," *Physical Review A*, vol. 74, no. 6, p. 063806, 2006.

[8] M. Wu, A. C. Hryciw, C. Healey, D. P. Lake, H. Jayakumar, M. R. Freeman, J. P. Davis, and P. E. Barclay, "Dissipative and dispersive optomechanics in a nanocavity torque sensor," *Phys. Rev. X*, vol. 4, p. 021052, 2014.